# The high strain rate response of UHMWPE: from fibre to laminate

B. P. Russell*, K. Kandan, V. S. Deshpande and N. A. Fleck
*Department of Engineering, Cambridge University,*
*Trumpington Street, Cambridge, CB2 1PZ, UK*
**Corresponding Author (bpr23@eng.cam.ac.uk) +441223 748541*

Keywords: high-speed deformation; tension test; fiber reinforced composites; fiber

## Abstract

The effect of strain rate upon the uniaxial response of Ultra High Molecular-weight Polyethylene (UHMWPE) fibres, yarns and laminates has been measured. Hot-pressed laminates, of lay-up $[0/90]_{48}$ and of volume fraction 83% UHMWPE fibres, 17% polyurethane (PU) matrix, were tested in both the 0/90° and ±45° configurations. The tensile strength of the matrix-dominated ±45° laminate is two orders of magnitude less than that of the fibre-dominated 0/90° laminate, and is more sensitive to strain rate. In order to obtain the high strain rate data, a dynamic test arrangement with piezoelectric force sensor device was developed, and this achieved a rise time of less than 1 μs. It is found that the failure strength (and failure strain) of the yarn is almost insensitive to strain rate within the range ($10^{-1}$ - $10^{3}$ $s^{-1}$). At low strain rates (below $10^{-1}$ $s^{-1}$), creep of the yarn dominates and the failure strain increases with diminishing strain rate. There is good correlation between the tensile strength of a laminate and that of dry yarn, once the volume fraction of loaded fibres in the laminate has been accounted for. The sensitivity of fibre and yarn strengths to grip condition was also explored, and the degree of knock-down in strength due to stress concentrations at the grips and to non-uniform fibre tension was quantified.

# 1. Introduction

Ultra High Molecular-weight Polyethylene (UHMWPE) in the drawn state is a crystalline polymer with an increasing range of structural application. Initial use in the 1950s was in the bulk form and included prosthetics for biomedical arthroplastic procedures. After its discovery in the late 1970s, fibres were commercialised by DSM Dyneema, NL under the trade name Dyneema®, thereby enabling the creation of high performance fabrics for use in sails, ropes and in long-fibre composite laminates for use in ballistic and blast armours. Much of the early characterisation on UHMWPE fibres was done at the University of Technology, Eindhoven. Jacobs et al. [1] comprehensively characterised the creep response while Govaert et al. [2] investigated the time-temperature correspondence of UHMWPE fibres. Peijs et al. [3] extended this work to laminates by first fabricating laminates from UHMWPE fibres and also reporting their mechanical properties with the aim of clarifying the potential of such composites for structural applications. An initial numerical study on the ballistic performance of UHMWPE fibre laminates was reported by Frissen et al. [4]. Since those initial studies, the uptake of Dyneema® based laminate materials by military organisations around the world is testament to its capability in the field; however, the mechanics by which these materials resist ballistic threats remains poorly understood.

A major step in understanding the ballistic performance of fibre composites was the experimental observation by Cunniff [5] that the critical velocity for penetration of armour fabrics by a projectile scales linearly with the so-called Cunniff velocity $c^*$ where

$$c^* \equiv \left(\frac{\sigma_f}{\rho}\right)^{1/2} \left(\frac{\varepsilon_f}{4}\right)^{1/6} \tag{1}$$

in terms of the tensile failure strength $\sigma_f$, failure strain $\varepsilon_f$ and density $\rho$ of the fibre. This scaling law was supported by the theoretical treatment by Phoenix [6], and reveals that $c^*$ is sensitive to the specific strength $\left(\sigma_f / \rho\right)^{1/2}$ but is only weakly dependent upon the tensile failure strain. Phoenix [6] argued that the deformation and failure of the target plate is dominated by membrane stresses and inertial effects (in the form of in-plane elastic waves). It is instructive to compare the values of $c^*$ for a range of ballistic materials, based upon single fibre tests [7-12]. The predicted values of $c^*$ in Table 1 are based upon tests performed at the highest strain rate $\dot{\varepsilon}$ available in the literature: this can have an important bearing upon the value of $c^*$ since creep effects can significantly depress $\sigma_f$ and elevate $\varepsilon_f$. It is clear from Table 1 that Dyneema® fibres are competitive for ballistic and blast applications. However, the pertinent strain rate in a ballistic test is on the order of $10^3$ $s^{-1}$ and so it is imperative to obtain high strain rate data for a meaningful comparison of performance to be made. This motivates the present study: our intent is to measure the high strain rate response of Dyneema® fibres in yarn form and to compare this response with that of a Dyneema® based laminate.

Table 1: List of some high strength fibres with the high strain rate failure stress, failure strain and the Cunniff velocity included.

| Fibre | $\rho$ (kg m$^{-3}$) | $\dot{\varepsilon}$ (s$^{-1}$) | $\sigma_f$ (GPa) | $\varepsilon_f$ (%) | $c^*$ (m s$^{-1}$) |
|---|---|---|---|---|---|
| Dyneema® [7] | 970 | 700 | 2.55 | 6.26 | 698 |
| Spectra 900 [8] | 970 | 433 | 2.5 | 3.0 | 689 |
| M5 [9] | 1700 | Not stated | 4.0 | 1.4 | 712 |
| Toray T1000 [10] | 1800 | Not stated | 6.4 | 2.2 | 947 |
| Toray T700 [11] | 1570 | 1000 | 3.4 | 1.57 | 665 |
| Kevlar 49 [12] | 1440 | 1350 | 3.08 | 3.86 | 650 |

Previous tests on UHMWPE laminates have suffered from the problem of load introduction into the gauge section. The fibre properties, as deduced from laminate tests, are significantly less than those implied by the fibre strength quoted in the literature [13-23]. There is a need to perform laminate tests that are free from these shortcomings, and to relate the laminate properties to the fibre properties. This is a second objective of the present study.

The outline of this paper is as follows. First, the microstructure of a 0/90° laminate of Dyneema® fibre laminate is reported. The laminate material is denoted HB26 by the manufacturer DSM Dyneema, and comprises SK76 fibres of volume fraction of 83% in a polyurethane (PU) matrix. The laminate was tested in the $[0/90]_{48}$ configuration and in the $[45/-45]_{48}$ configuration, in uniaxial tension at low strain rates in the range $10^{-4}$ s$^{-1}$ to $10^{-2}$ s$^{-1}$. Second, the stress versus strain response of dry yarns were measured over a wide range of strain rate, $10^{-4}$ s$^{-1}$ to $10^{3}$ s$^{-1}$. In order to explore the role of fibre waviness/twist upon yarn strength, an additional set of tests were performed on single fibres at a strain rate of $10^{-3}$ s$^{-1}$.

## 2. The microstructure and properties of the laminate

The HB26 laminate was made by hot-pressing of UHMWPE fibres, each of diameter 17 μm, in a PU matrix to give a $[0/90]_{48}$ lay-up with a ply thickness of 60 μm. The processing steps are shown in Fig. 1 and are summarised as follows.

Step I: Fibres are produced through a gel-spinning/hot drawing process [24,25]. The UHMWPE is dissolved in a solvent at a temperature of 150°C. The solution is pumped through a spinneret with a few hundred capillaries to form liquid filaments which are then quenched in water to form a gel-fibre. The gel-fibre is then drawn at a strain rate on the order of 1 s$^{-1}$ in hot air (at 120°C), resulting in a highly orientated and highly crystalline fibre of diameter 17 μm. Draw ratios for Dyneema® fibres are typically a factor of 30 or more in order to achieve the desired mechanical properties.

Step II: Fibres are coated in a PU resin solution and are then formed into a [0/90/0/90] stack. A drying process removes the PU matrix solvent from the stack, and the stack is treated as an intermediate product from which laminate plates can be made.

Step III: The [0/90/0/90] stack is cut, laid-up to the required thickness and hot pressed (the details are proprietary to DSM). Bonding of the layers is achieved through partial melting of the PU matrix material. The fibre diameter is unchanged by the hot-pressing operation, although a proportion of the fibres change their cross-sectional shape, as detailed below.

## 2.1 Microstructure of the laminate

Microscopic examination of the fibre and matrix within a ply is made difficult by the phenomenon of smearing of the surface during specimen preparation by polishing or cutting. Smearing is a distortion of the surface profile, exaggerating some features and suppressing others; it arises from the low shear strength and low cohesive strength of fibre and matrix. The following preparation steps were taken to overcome this problem, and thereby allow for the generation of representative micrographs. An edge view of the $[0/90]_{48}$ laminate was obtained by mounting a sample in moulding epoxy (Di-hard, produced by MetPrep[1]), followed by hand grinding down to 4000 grit using SiC paper. The sample was polished using a short-napped cloth (Trounoire M, produced by Metprep) and progressively finer suspensions of $\alpha$-$Al_2O_3$ particles down to 300 nm, and then a colloidal silica of particle size 40 nm. The surface was etched by concentrated sulphuric acid to remove excess polyurethane and the specimen was re-polished using the 40 nm colloidal silica.

Optical microscopy was used in order to examine the fibre arrangement within each ply, see Fig. 2a for bright field and Fig. 2b for dark field. It was found that bright field microscopy (and likewise SEM observation) of the as-polished surface is misleading due to the presence of a very thin layer of smeared matrix and fibre material (of thickness on the order of a few microns). To obviate this problem, dark field microscopy was used, see Fig. 2b. The dark field image gives better contrast between fibre and matrix and reveals more clearly the cross-sectional shape of the fibre.

The laminate is comprised of orthogonally alternating plies, each with a thickness of approximately 60 µm. Zones of close-packed fibres are evident within each ply: the clumped fibres are of hexagonal cross-section due to the hot pressing operation. Between these zones, the fibres remain separated by matrix and are approximately circular in cross-section.

A similar compaction phenomenon occurs at the cross-over points between orthogonal plies, see Fig. 3. The figure shows the delamination surface due to peeling of one layer from the next. Brinelling (indentation) of the fibres occurs at the contact sites between orthogonal fibres; two representative sites are labelled B in Fig. 3. The matrix between adjacent plies is also evident as a continuous, but perforated sheet: the holes in this matrix sheet are associated with the cross-over points between orthogonal fibres. The degree of adhesion between matrix and fibre is poor as the peeling process was achieved manually and induced minimal damage to fibre and matrix.

[1] MetPrep, Curriers Close, Charter Avenue, Coventry CV4 8AW

## 2.2 Tensile tests on the laminate

Tensile tests were performed on the HB26 laminate in the $0°/90°$ and ±45° orientations, at strain rates in the range $10^{-4}$ $s^{-1}$ to $10^{-2}$ $s^{-1}$. The properties of the composite preclude the use of standard test methods for determining the tensile response. It is highly anisotropic with a high strength along the fibre direction, and a low shear strength. Additionally, the composite has a low coefficient of friction, making grippage difficult. A dog-bone specimen was designed to introduce high axial stresses into the gauge section without triggering pull-out from the gripped (through-bolted) portion of the specimen by shear, see Fig. 4. The tensile tests were performed using a screw-driven test machine at fixed displacement rate, and the axial force on the specimen was measured directly with the load cell of the test machine. Axial nominal strain was measured using a clip gauge of gauge length 12.5 mm.

The measured uniaxial tensile response of the $0°/90°$ HB26 laminate is shown in Fig. 5a, for selected strain rates in the range of $10^{-4}$ $s^{-1}$ to $10^{-2}$ $s^{-1}$. The response of the specimens at different strain rates is consistent with a viscoelastic/activated creep material response as was proposed by Wilding and Ward [18]. At the lowest strain rate, $\dot{\varepsilon} = 10^{-4}$ $s^{-1}$, an initial non-linear behaviour is observed, and on unloading from approximately 600 MPa to zero load (solid line Fig. 5a) there is a residual strain of 0.5%. As the strain rate is increased, the response becomes more linear, and the strain to failure decreases. The peak strength of 725 MPa is independent of strain rate over the range tested.

The tensile response of the ±45° lay-up is shown in Fig. 5b, for the same regime of strain rates. Note that the stress levels in these tests is more than two orders of magnitude less than that of the $0°/90°$ specimens; this is due to the fact that tensile tests on the ±45° lay-up probes the shear response of the fibres and matrix (the ratio of gauge length to gauge width of the specimen was about 10 and thus we anticipate deformation to occur by scissoring of the fibres rather than by axial tensile deformation of the fibres). A yield point is observed in the ±45° lay-up at an axial stress level of approximately 7 MPa. Post-yield, the strength increases and this is associated with orientation-hardening: as the fibres rotate towards the loading axis, the response stiffens as an increasing contribution of the axial load is carried by the elastic fibres. Failure occurs at an axial stress of 12-17 MPa, depending upon strain rate, and at a strain level on the order of 0.2 (note that this failure strain exceeds that of the $0°/90°$ laminate by an order of magnitude). Failure of the ±45° lay-up occurs in the matrix, and gives rise to a characteristic 'chevron' pattern at the macroscopic level, see Fig. 6. At failure, the fibres remain intact but the included angle between fibres in adjacent plies has reduced from 90° to 74°, see Fig. 6b, indicating that each ply has undergone a rotation of 8° toward the loading axis. This finite rotation gives rise to the orientation hardening as already mentioned above.

It is a formidable challenge to measure the high strain rate tensile response of the laminate as the low shear strength of the composite makes it difficult to introduce axial stress into the laminate. Consequently, we adopt the pragmatic approach of measuring the high strain rate tensile response of the yarn, and use this to infer the laminate response at high strain rates.

# 3. Measurements of the tensile properties of yarns

We describe below a test method that was used to measure the tensile response of the Dyneema® SK76 yarn over an extremely wide range of strain rates in the range $10^{-4}$ $s^{-1}$ to $10^{3}$ $s^{-1}$. We emphasise

that the same test arrangement was used for all strain rates in order to allow for a direct assessment of the sensitivity of response to strain rate.

## 3.1 Test arrangement

The as-received material is a spool of yarn consisting of 780 fibres, with no twist. A dynamic test method has been developed in order to measure the tensile stress versus strain response of yarn, of gauge length 5-20 mm, see Fig. 7. Yarn is wrapped around a semi-circular anvil to form two nominally identical test samples. The precise test procedure is different for high strain rates (above 100 $s^{-1}$) and for low strain rates.

***(a) High strain rate tests (above 100 $s^{-1}$)***

The principle of operation of the high strain rate tests is to stretch the yarns impulsively by impact of the gripping anvil (Fig. 7) by a relatively heavy projectile at velocities in the range 4–50 $ms^{-1}$. The tests are performed at fixed strain rate as dictated by the impact velocity (and yarn length). The axial strain (and strain rate) in the yarn is measured by marking a gauge length on the yarn (in the range 4-16 mm) with a marker pen, and using a high speed camera in order to measure the transient separation of the two marks, see Fig. 7b. Digital image correlation was used to post-process the high speed images, by identifying the location of the inner edges of the 2 marker bands. This method gave an accuracy of 0.1% in axial strain of the yarn.

The force in the yarn is measured via a piezoelectric force sensor[2] of rise time $< 1$ µs. It was modified by bonding a titanium grip and steel pin of diameter 2 mm directly to the force sensor diaphragm using an epoxy adhesive[3]. The combined mass of sensor diaphragm and grip equals 3.55 x $10^{-4}$ kg, and the axial stiffness of the sensor is $s = 130$ $GNm^{-1}$. Upon treating the sensor and grip as a mass-spring system, we infer a period of free oscillation of

$$T = 2\pi\sqrt{\frac{m}{s}} = 0.33\ \mu s \qquad (2)$$

This period is comparable to the elastic wave propagation time of 0.5 µs for the yarn specimens of length 5 mm, as used in the highest rate tests. For comparison, the test time at $\dot{\varepsilon} = 10^3$ $s^{-1}$ is on the order of 20 µs. Consequently, we can assume that axial equilibrium is established in all of the high strain rate tests and that the response of the force sensor is sufficiently decoupled from the fibre response.

It is worth noting that for a practical specimen length of 5 mm, the elastic transit time prohibits the material response from being captured much beyond strain rates of $10^3$ $s^{-1}$. This can be made precise as follows. The maximum strain rate to achieve an accurate material response is set by equating the test time $t_f$ to the time for force equilibrium $t_e$ within the sample. The test time $t_f$ is related to the applied strain rate $\dot{\varepsilon}$ and to the failure strain $\varepsilon_f$ according to $t_f = \varepsilon_f/\dot{\varepsilon}$. The time for the establishment of axial equilibrium is taken to be the time for 10 wave reflections, $t_e = 10\ell/c$, for a yarn of length $\ell$ and axial wavespeed $c$. Upon equating these two time-scales, we obtain a

[2] product reference 113B24, PCB Piezotronics Inc, 3425 Walden Avenue, Depew, New York 14043-2495 USA
[3] Redux 810, Hexcel Composites, 281 Tresser Boulevard, 16th Floor, Stamford, CT 06901-3261, USA

limiting strain rate of $\dot{\varepsilon} = \varepsilon_f c/(10\ell)$. Now substitute for some typical values, $\varepsilon_f$ = 2%, $c$ = $10^4$ ms$^{-1}$, $\ell$ = 5 mm, to give $\dot{\varepsilon} = 4000$ s$^{-1}$.

The yarn samples were manufactured by the following procedure in order to ensure repeatable results.

(i) The initial location of the loading anvil with respect to the force sensors is defined by an end-stop on the anvil. This sets the gauge length of the yarn, and ensures that both samples are equally loaded during the tests.

(ii) Yarns consisting of 175 – 200 fibres are fastened to an anchor pin A on the anvil (Fig. 7a) by a tying a knot and then applying cyanoacrylate adhesive to the knot.

(ii) The yarn is wrapped around the semi-circular face of the anvil and adhered to it by the cyanoacrylate adhesive. The free end of the yarn is then looped around the pin of force sensor B, and brought back to the anvil.

(iii) The yarn is wrapped back over the semi-circular face of the anvil, and adhered to it by the adhesive. The free end of the yarn is looped around the pin of force sensor A, and brought back to the anvil.

(iv) Finally, the end portion of the yarn is wrapped over, and adhered to, the semi-circular face of the anvil, and knotted to the anchor pin B of the anvil.

***(b) Low strain rate tests (below 100 s$^{-1}$)***

The low strain rate tests involve anvil velocities of less than 1 mm s$^{-1}$, and to achieve this, the anvil was fastened to the cross-head of a servo-hydraulic test machine via a loading rod, with 100 N conventional load cell in tandem. The axial strain was measured both by the high speed camera (and these measurements were verified by the LVDT on the machine cross-head).

At strain rates below $10^2$ s$^{-1}$, the piezo force sensors were inaccurate due to charge loss from the device (with a time constant of 10 s) and were disregarded for force measurement. At the strain rate of $10^2$ s$^{-1}$ both the piezo force gauges and load cell give accurate measurements and in agreement with each other.

## 3.2 Discussion of the dynamic results

The tensile response of the yarn is quoted in terms of the average tensile stress versus strain response of each fibre comprising the yarn. The axial stress in a fibre is deduced from: (i) the force on the yarn, (ii) the number of fibres per yarn (780), and (iii) the cross-sectional area of each fibre. In order to obtain the cross-sectional area of a fibre, the linear density of the yarn was measured and thereby the linear density of each fibre determined to be 2.20 x $10^{-7}$ kg m$^{-1}$. The fibres were assumed to have a circular cross section and uniform density $\rho$ = 970 kg m$^{-3}$, and the inferred diameter of each fibre is then $D$ = 17.0 μm. Direct measurement of the fibre diameter in the SEM gave good agreement with this value.

Representative stress versus strain curves for Dyneema® SK76 yarns are shown in Fig. 8a for strain rates $\dot{\varepsilon}$ in the range $10^{-4}$ s$^{-1}$ to $10^3$ s$^{-1}$. The response is strain rate dependent at low strain rates (below $10^{-1}$ s$^{-1}$), and this attributed to creep of the Dyneema® fibres [18]. In contrast, at $\dot{\varepsilon} \geq$

$10^{-1}s^{-1}$, the stress versus strain response of the fibres is linear to failure and the curves collapse onto each other.

It is instructive to plot the dependence of the peak stress $\sigma_f$ and failure strain $\varepsilon_f$ and Young's modulus *E* of the yarns as a function of strain rate; see Figs. 8b, c and d, respectively. Here, failure strain is defined as the strain at peak stress. Literature values for ultra high molecular weight polyethylenes are included in the figures: data for Spectra 900 [8], Dyneema® SK75 [22], Dyneema® SK75 [23]. Koh et al. [7] also performed tests on a Dyneema®, although the precise fibre type was not specified in that study. These earlier studies are each limited to a more restrictive range of strain rate. Consider first, the strength data in Fig. 8b. There is good agreement between the results of the present study and earlier observations. In contrast, the failure strain $\varepsilon_f$ is close to 2% in the present study (for strain rates exceeding $10^{-2}$ $s^{-1}$), whereas the corresponding failure strains from the literature exceed 4%. The discrepancy is largely explained by the fact that the strain measurements in previous studies are not based upon the elongation of a gauge length on the specimen. Rather, the relative displacement of loading grips is used, and slip between specimen and grips has not been accounted for. For the same reason, the literature values of Young's modulus are much lower values than those reported in the present study (35-80 GPa compared with 130 GPa).

## 3.3 Comparison of yarn and laminate tensile responses

It is instructive to compare the measured tensile response of the $[0/90]_{48}$ laminate with that of the yarn at low strain rates. (It was not possible to test the laminate at high strain rate.) We begin by arguing that the contribution to macroscopic modulus from the 90° plies is negligible compared to that of the 0° plies in the $[0/90]_{48}$ laminate. The macroscopic modulus from the 90° plies is of similar magnitude to that of the tensile modulus of a ±45° lay-up; the data given in Fig. 5b reveals an initial modulus of 800 MPa. In contrast, the axial modulus of the yarn is on the order of 130 GPa: a difference of 2 orders of magnitude. Consequently, we can assert that the tensile response of the $[0/90]_{48}$ laminate is dominated by that of the fibres in the 0° plies. The axial stress in the 0° fibres is given by

$$\sigma = \frac{2\sigma_L}{V_f} \tag{3}$$

where $\sigma_L$ is the nominal stress over the cross-section of the $[0/90]_{48}$ laminate and the fibre volume fraction $V_f$ is taken to be 83%. The resulting comparison of stress versus strain response of loaded fibres in the $[0/90]_{48}$ laminate and in the yarn is shown in Fig. 9 for strain rates in the range $10^{-4}$ $s^{-1}$ to $10^{-2}$ $s^{-1}$. There is excellent agreement for the measured values of initial modulus. In contrast, the failure strength of the yarn is 20 % greater than the laminate and the failure strain is 30 - 50% greater. This may be attributed to the fact that the processing route of the laminate involves an additional hot-pressing operation.

## 3.4 Comparison of yarn and single fibre tensile responses

We proceed to compare the measured yarn strength of 2.2 GPa at low strain rate ($10^{-3}$ $s^{-1}$) with the quoted value[4] for a single fibre of 3.59 GPa [26]. The discrepancy is significant and possible reasons for this are as follows:

(i) the roller diameter of 2 mm is sufficiently small in the yarn tests to introduce significant stress concentrations.

(ii) the steel rollers lead to abrasion of the yarn and thereby to premature failure

(iii) the fibres within the yarn may not be loaded uniformly due to waviness of the fibres.

We investigate each possibility in turn.

(i) In order to assess the level of stress concentration introduced into the yarn by the rollers, an additional set of tests was performed with the roller diameter varied from 2 mm to 175 mm. The yarn strength increases slightly with increasing roller diameter, see Fig. 10, such that the yarn strength equals 2.5 GPa for a roller of diameter 175 mm. We conclude that the stress concentration as introduced by the rollers is minor.

(ii) In order to determine whether abrasion of the yarn surface by the steel rollers leads to a knock-down in strength, an additional test was performed on yarn bonded to rubber loading tabs, as follows. The yarn was sandwiched between two rubber sheets and bonded to them using cyanoacrylate adhesive, as shown in Fig. 11a; the rubber face-sheets were then friction gripped in the serrated jaws of a screw-driven test machine. The axial load in the yarn was measured by the load cell of the test machine, while the axial strain was measured by digital image correlation of the separation between two marks on the yarn; this technique was identical to that used in the roller tests. The observed tensile response of the yarn is compared in Fig. 11b with that for the roller-gips, as taken from Fig. 8a. We note that the initial modulus is the same for the two yarn tests but the failure strength has increased from 2.2 GPa to 3.0 GPa when the grips are changed from steel rollers to rubber pads. We conclude that the tensile strength of the yarn is somewhat sensitive to the elastic modulus of the grips in contact with the yarn.

(iii) The strength of 3.0 GPa for the rubber-gripped yarn is still less than the value of 3.59 GPa, as reported for a single fibre [26]. This discrepancy could be due to fibre waviness within the yarn, or it could be due to the fact that the quoted value of 3.59 GPa exceeds the actual fibre strength for the batch of material tested herein. To resolve this, a final test was performed, such that the single fibre was adhered to rubber tabs and tested in tension, as described in (ii) above. The observed tensile response is included in Fig. 11b. The observed single fibre strength equals 3.8 GPa, in support of the quoted value of 3.59 GPa. Hence, the presence of waviness within the yarn leads to non-uniform loading of the yarn, and is the explanation for the drop in strength from 3.8 GPa to 3.0 GPa. We

[4] Data sheet values for fibres strengths is usually quoted in units of N/tex; these units are equivalent to stress in units of GPa divided by density in units of g $cm^{-3}$. The strength of single fibres of SK76, is 3.7 N/tex, equivalent to 3.59 GPa [26].

further note that extreme measures have had to be taken in order to reproduce the strengths as quoted in [26]. Practical Dyneema® laminates display tensile strengths in agreement with the yarn strengths as tested by rollers.

## 4. Conclusions

The present study has elucidated the relationship between the tensile properties of the laminate, yarn and fibre for Dyneema® SK76 over a wide range of strain rate. Tests on the yarn demonstrate an insensitivity of response to strain rate in the range of $10^{-2}$ $s^{-1}$ to $10^{3}$ $s^{-1}$. (In order to acquire the high strain data, extreme care was needed in the test protocol, and in the use of instrumentation for both force and strain measurement.) At strain rates below $10^{-2}$ $s^{-1}$ creep effects become important, with a drop in modulus and tensile strength, and an increase in failure strain, recall Fig. 8. The tensile strength of a single fibre exceeds that of the yarn by about 20% due to the presence of fibre waviness within the yarn. Similarly, the strength of the yarn exceeds that of 0° plies in a $[0/90]_{48}$ laminate by about 20%, and this is ascribed to differences in processing route.

## Acknowledgement

The authors are grateful for financial support from the US Office of Naval Research (contract N62909-10-1-7122). They wish to thank DSM Dyneema for supplying the SK76 yarn and the HB26 laminate plates. Dyneema® is a trademark of DSM. Dr B. P. Russell was supported by a Ministry of Defence / Royal Academy of Engineering Research Fellowship.

## References


[1] Jacobs M, Heijnen N, Bastiaansen C, Lemstra PJ. Macromol Mater Eng 2000;283:120

[2] Govaert LE, Lemstra PJ. Colloid Polym Sci 1992;270:455

[3] Peijs A, Catsman P, Govaert LE, Lemstra PJ. Composites 1990;21:513

[4] Frissen RJT. Modelling the Ballistic Impact Behaviour of Polyethylene-Fibre-Reinforced Composites. Eindhoven: University of Technology; 1996

[5] Cunniff PM. Dimensionless parameters for optimization of textile-based body armor systems, in: Reinecke WG (Ed.). Proceedings of the 18th International Symposium on Ballistics, San Antonio, TX. Lancaster: Technomic; 1999

[6] Phoenix SL. Int J Solids Struct 2003;40:6723

[7] Huang W, Wang Y, Xia Y. Polym 2004;45:3729

[8] Koh ACP, Shim VPW, Tan VBC. Int J Impact Eng 2010;37:324

[9] Cunniff PM, Auerbach MA, Vetter E, Sikkema DJ. High Performance M5 fiber for ballistics/structural composites, in: Proceedings of the 23rd Army Science Conference; Orlando, FL; 2002

[10] Manufactures data sheet: Toray T1000, Toray, Japan.

[11] Zhou Y, Wang Y, Xia Y, Jeelani S. Mater Letters 2010;64:246

[12] Wang Y, Xia YM. Composites Part A 1999;30:1251

[13] Benloulo IC, Rodriguez J, Martinez MA, Galvez VS. Int J Impact Eng 1997;19:135

[14] Morye SS, Hine PJ, Duckett RA, Carr DJ, Ward IM. Composites Part A 1999;30:649

[15] Koh C, Shim V, Tan V, Tan B. Int J Impact Eng 2008;35:559

[16] Capaccio G, Ward IM. (1974). Polym 1974;15:233

[17] Peijs T, Jacobs MJN, Lemstra PJ. High Performance Polyethylene Fibers, in: Kelly A, Zweben C (Eds.). Comprehensive Composite Materials. Pergamon; 2000

[18] Wilding M, Ward IM. Polym 1978;19:969

[19] Wilding M, Ward IM. Polym 1981;22:870

[20] Wilding MA, Ward IM. J Mater Sci 1984;19:629

[21] Govaert LE, Bastiaansen C, Leblans P. Polym 1993;34:534

[22] Kromm F, Lorriot T, Coutand B, Harry R, Quenisset JM. Polym Test 2003;22:463

[23] Dessain B, Moulaert O, Keunings R, Bunsell AR. J Mater Sci 1992;27:4515

[24] Smith P, Lemstra PJ, Kalb B, Pennings AJ. Polym Bull 1979;1:733

[25] Smith P, Lemstra P. J Mater Sci 1980;15:505

[26] Hearle JWS. High-performance fibres. Woodhead Publishing; 2001

## Figure Captions

Fig. 1: Sketch of the processing steps in the manufacture of the HB26 laminate material. Step I: fibres are first produced through gel-spinning and hot drawing, Step II: plies are fabricated through resin application and fibre alignment, Step III: cut sheets of ply are stacked and pressed under temperature to produce the final consolidated product.

Fig. 2: Optical images showing the ply structure at a fixed location in HB26 using (a) bright field and (b) dark field microscopy.

Fig. 3: SEM image showing brinelling of fibres (examples labelled B). Perforations within the matrix confirm that orthogonal fibres are in direct contact at the ply interface.

Fig. 4: Geometry of the tensile test specimen for the HB26 laminate.

Fig. 5: Stress-strain response of (a) 0/90° and (b) ±45° HB26 laminate performed at selected low strain rate values.

Fig. 6: Micrograph showing the fracture mechanism in a ±45°HB26 laminate tensile specimen.

Fig. 7: Experimental set up for yarn testing at high strain rates. (a) plan view and (b) side view.

Fig. 8: (a) Selected stress versus strain responses over a wide range of strain rates. Dependence of (b) peak strength, (c) failure strain and (d) initial modulus upon strain rate. Data from the literature for UHMWPEs is included in plots (b)-(d).

Fig. 9: Comparison of the stress versus strain responses for the SK76 yarn and HB26 laminate.

Fig. 10: SK76 yarn tests using a range of roller diameters. (a) Test set-up, (b) fibre strength versus roller diameter, $D$ for a test strain rate of $10^{-3}$ $s^{-1}$. Data from rubber-tabbed specimens are included for a single fibre and a yarn.

Fig. 11: (a) Sketch of the rubber end tab used for single fibre and yarn tensile tests. (b) The corresponding measured stress versus strain responses at a strain rate of $10^{-3}$ $s^{-1}$.

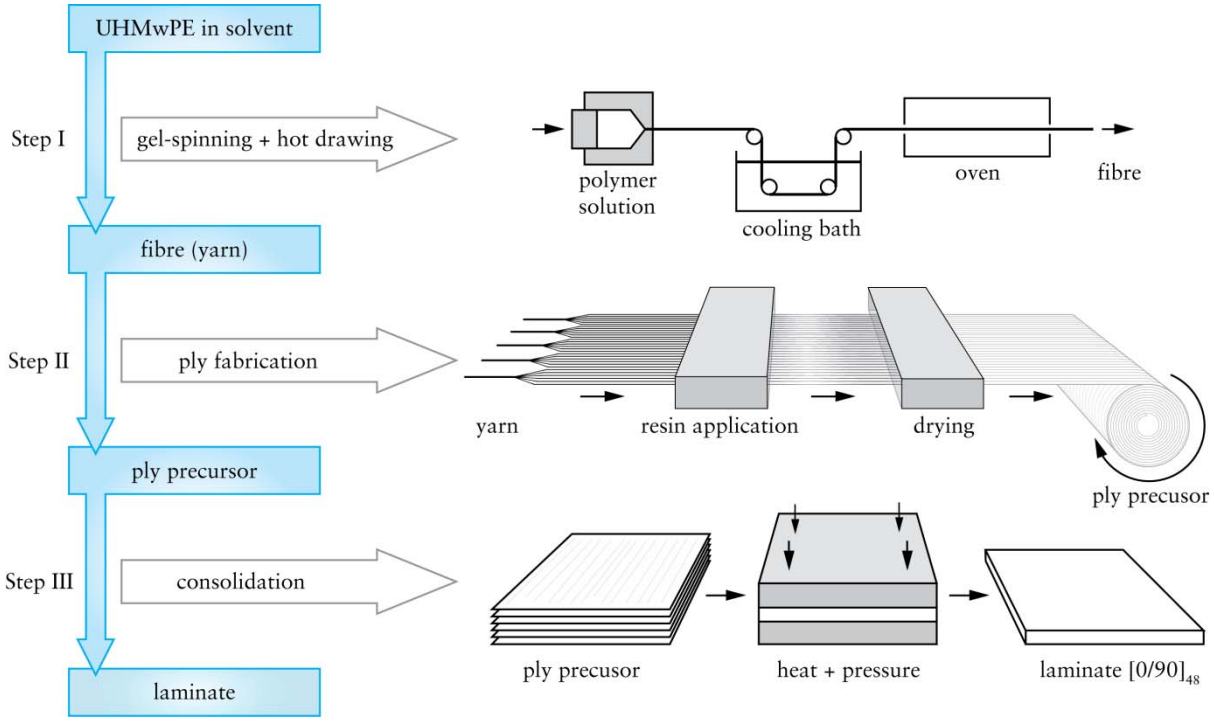


Fig. 1: Sketch of the processing steps in the manufacture of the HB26 laminate material. Step I: fibres are first produced through gel-spinning and hot drawing, Step II: plies are fabricated through resin application and fibre alignment, Step III: cut sheets of ply are stacked and pressed under temperature to produce the final consolidated product.

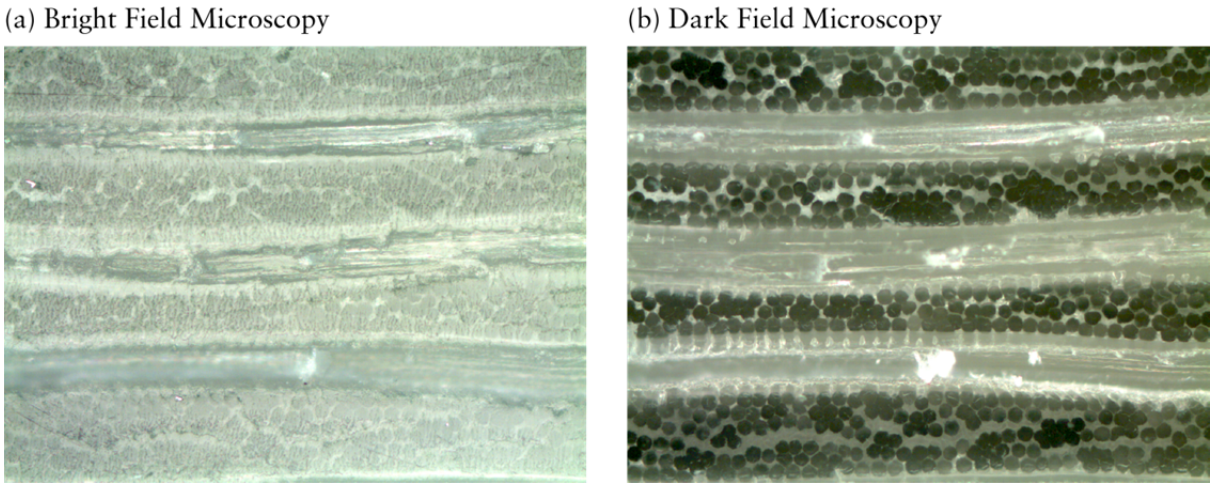


Fig. 2: Optical images showing the ply structure at a fixed location in HB26 using (a) bright field and (b) dark field microscopy.

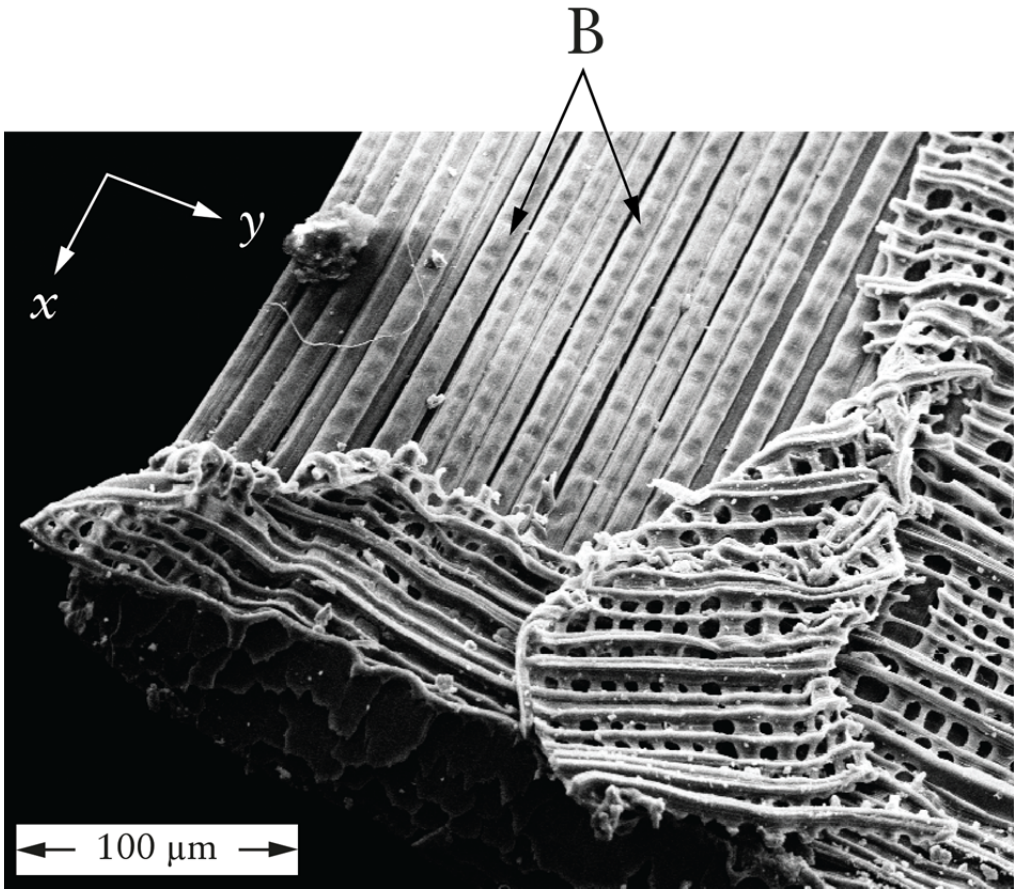


Fig. 3: SEM image showing brinelling of fibres (examples labelled B). Perforations within the matrix confirm that orthogonal fibres are in direct contact at the ply interface.

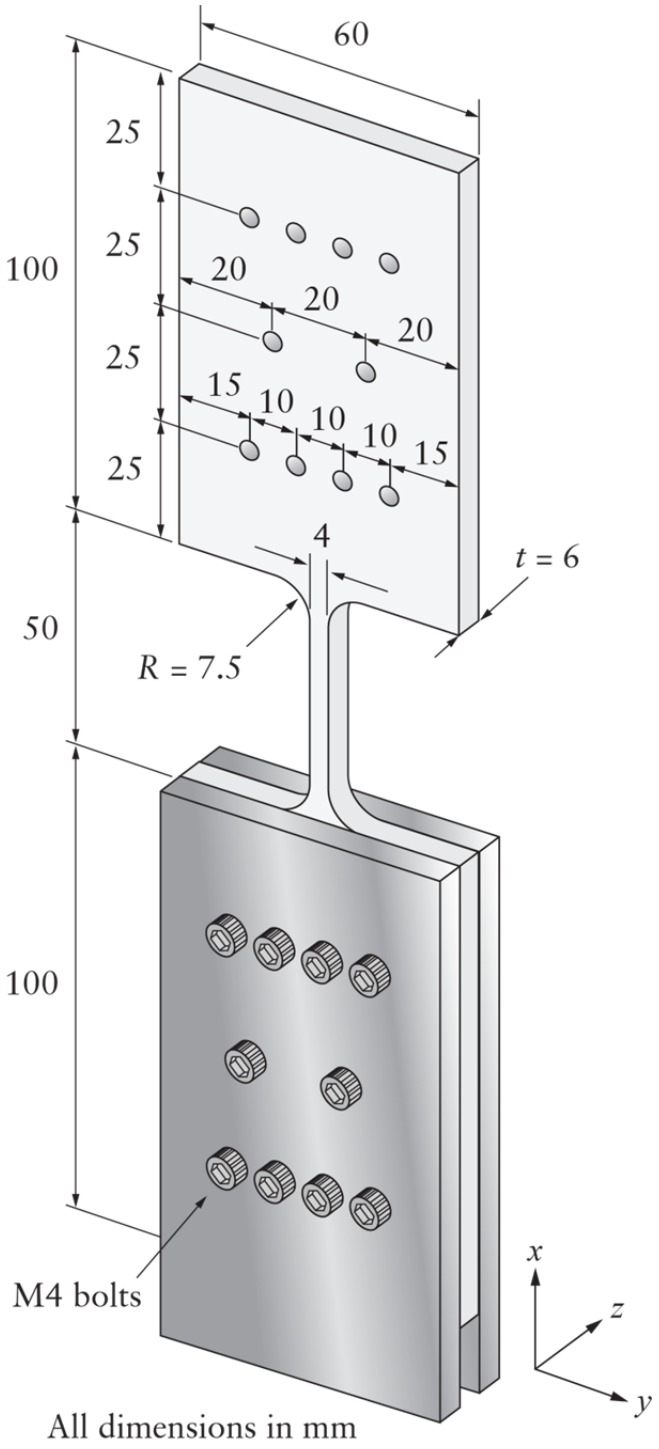


Fig. 4: Geometry of the tensile test specimen for the HB26 laminate.

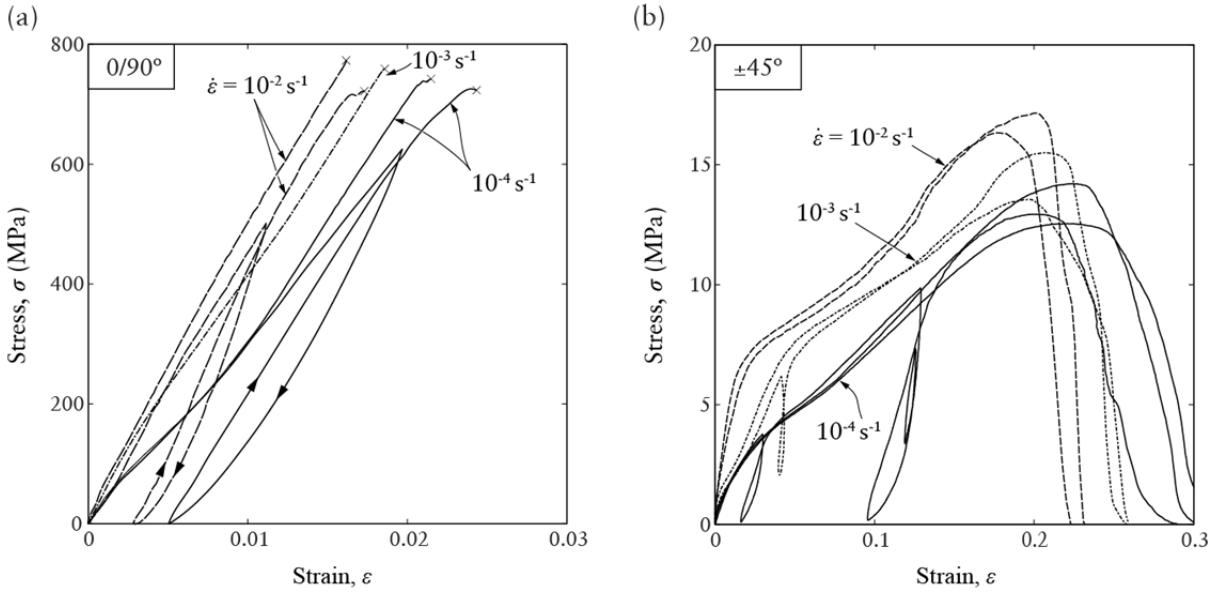


Fig. 5: Stress-strain response of (a) 0/90° and (b) ±45° HB26 laminate performed at selected low strain rate values.

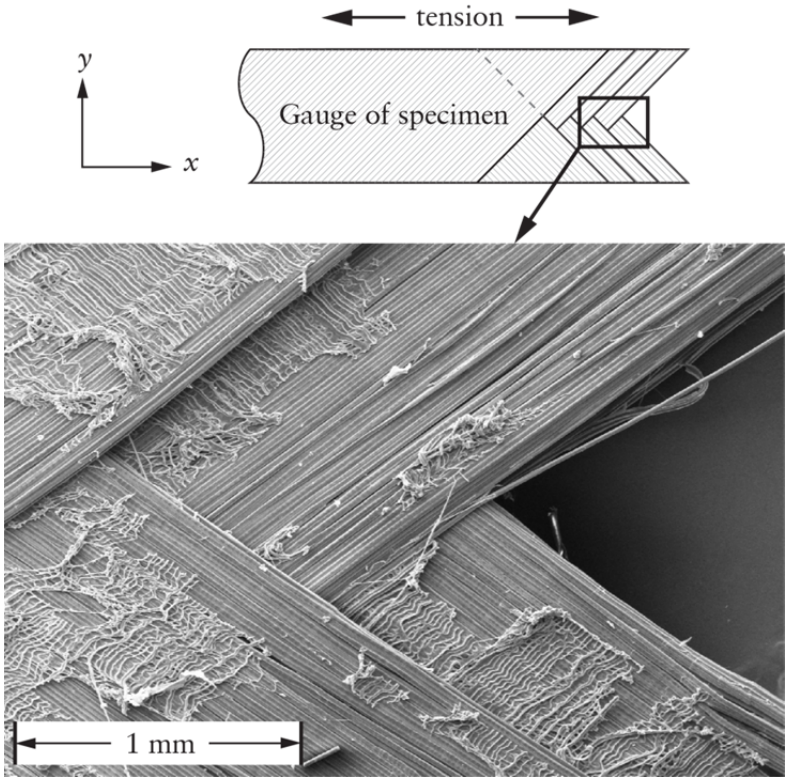


Fig. 6: Micrograph showing the fracture mechanism in a ±45°HB26 laminate tensile specimen.

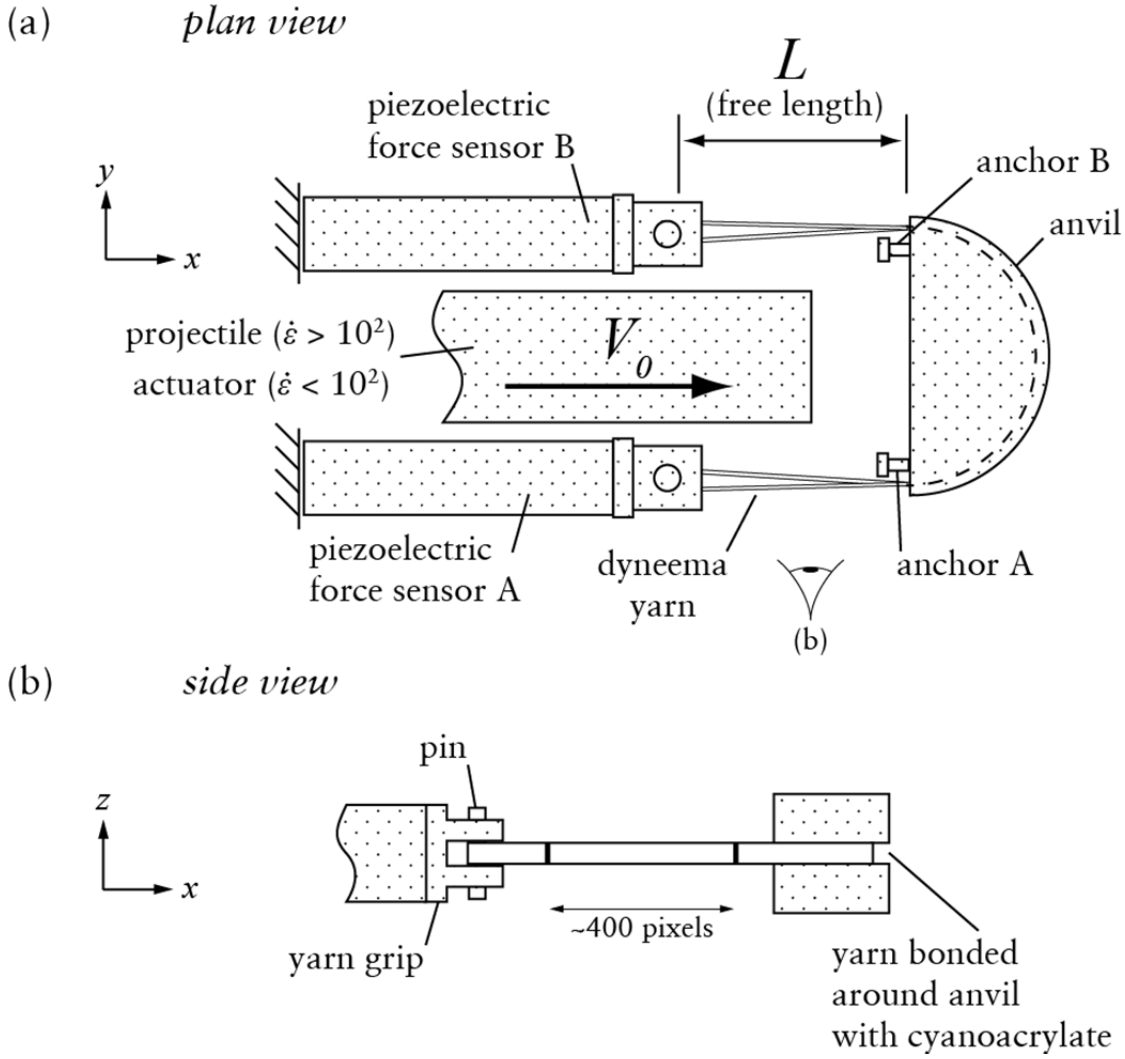


Fig. 7: Experimental set up for yarn testing at high strain rates. (a) plan view and (b) side view.

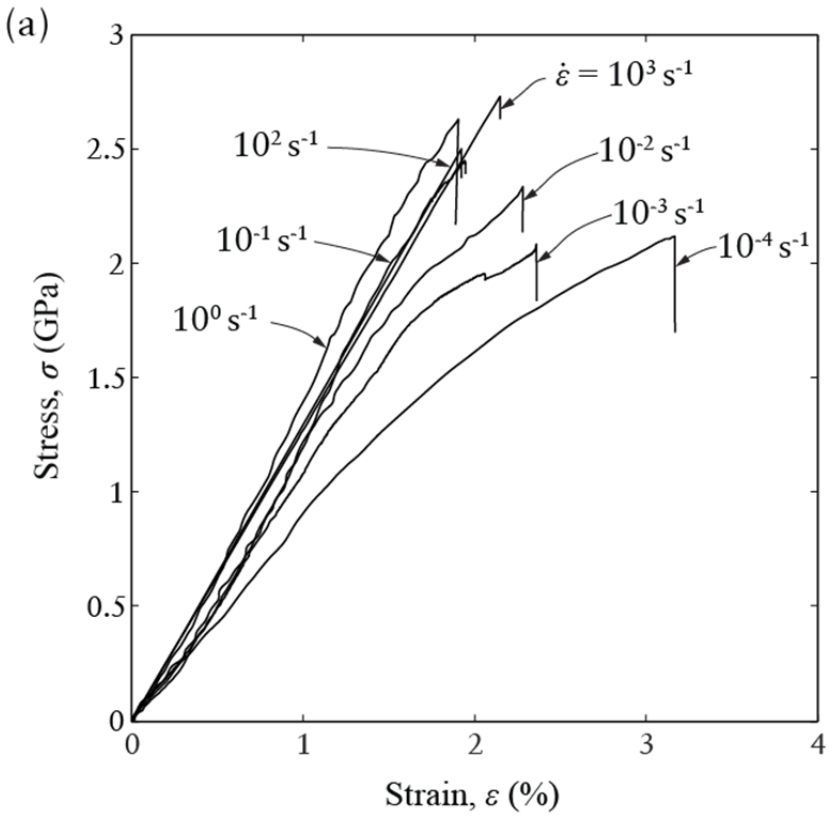
(a)
$\dot{\varepsilon} = 10^3\ s^{-1}$
$10^2\ s^{-1}$
$10^{-2}\ s^{-1}$
$10^{-1}\ s^{-1}$
$10^{-3}\ s^{-1}$
$10^{-4}\ s^{-1}$
$10^0\ s^{-1}$
Stress, $\sigma$ (GPa)
Strain, $\varepsilon$ (%)
0
0.5
1
1.5
2
2.5
3
4

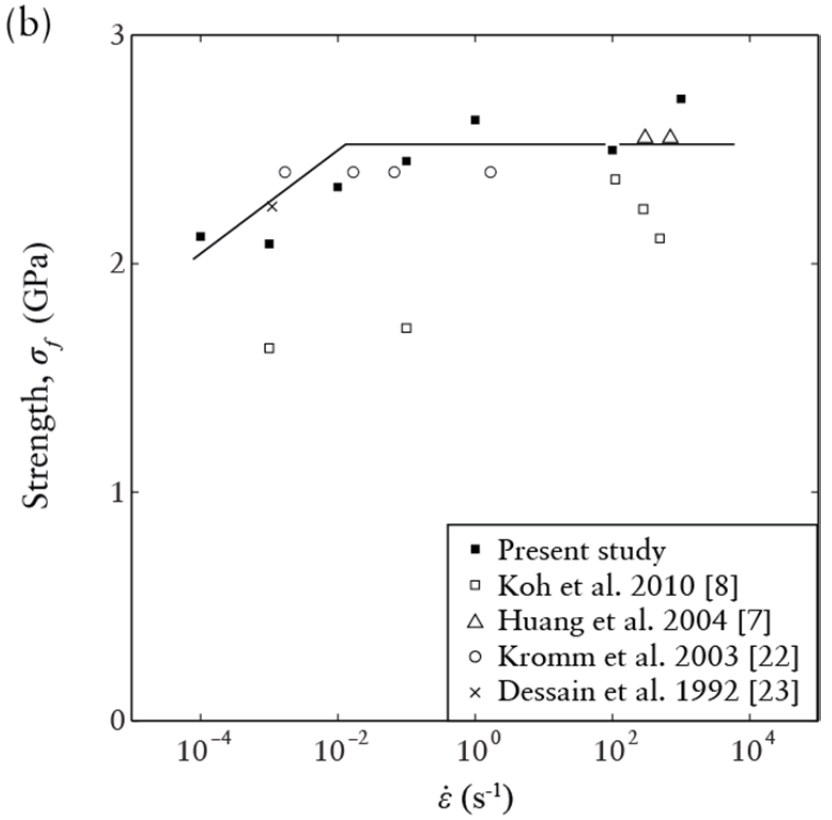
(b)
Present study
Koh et al. 2010 [8]
Huang et al. 2004 [7]
Kromm et al. 2003 [22]
Dessain et al. 1992 [23]
Strength, $\sigma_f$ (GPa)
$\dot{\varepsilon}$ ($s^{-1}$)
$10^{-4}$
$10^{-2}$
$10^{0}$
$10^{2}$
$10^{4}$
0
1
2
3

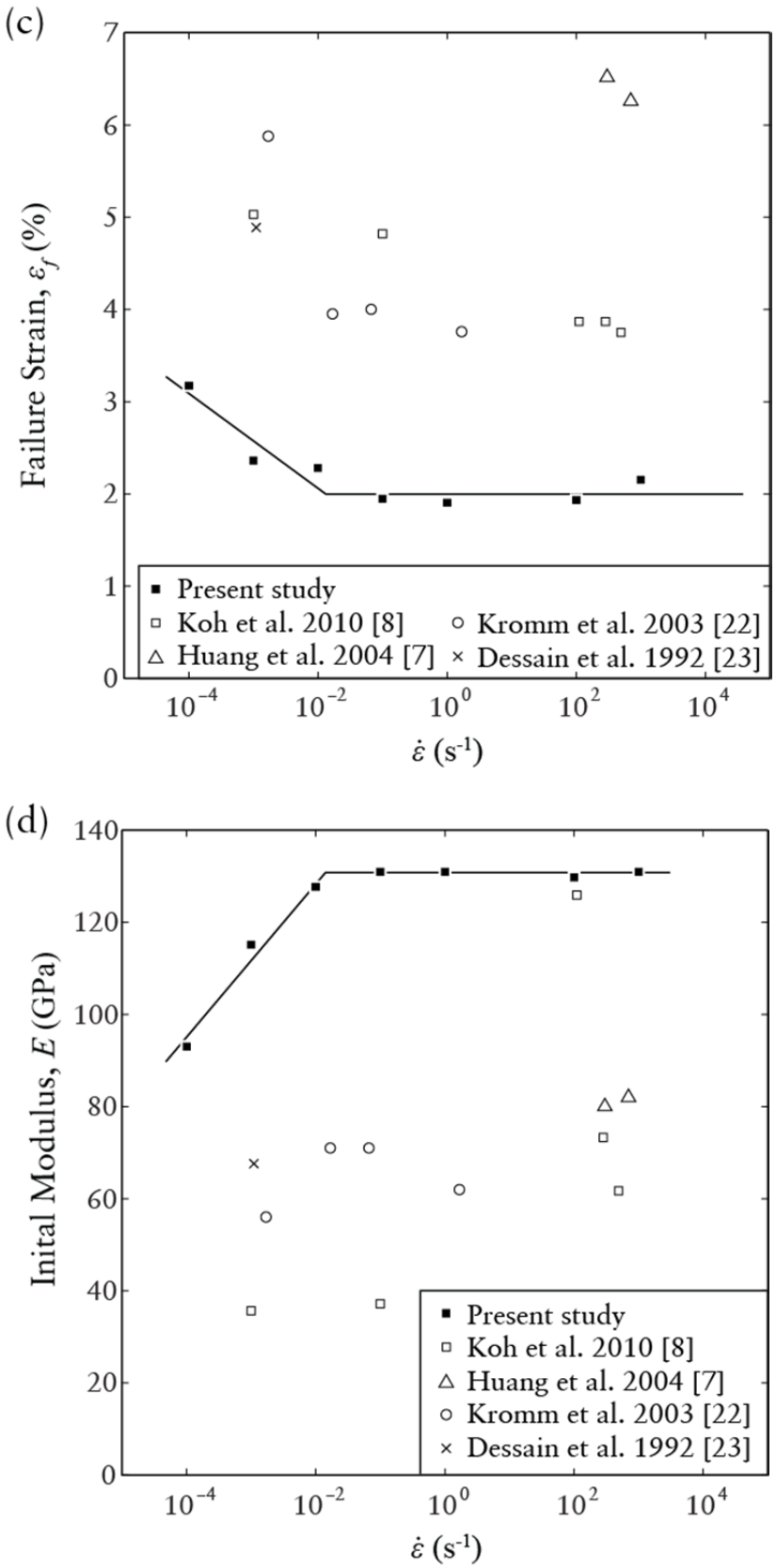


Fig. 8: (a) Selected stress versus strain responses over a wide range of strain rates. Dependence of (b) peak strength, (c) failure strain and (d) initial modulus upon strain rate. Data from the literature for UHMWPEs is included in plots (b)-(d).

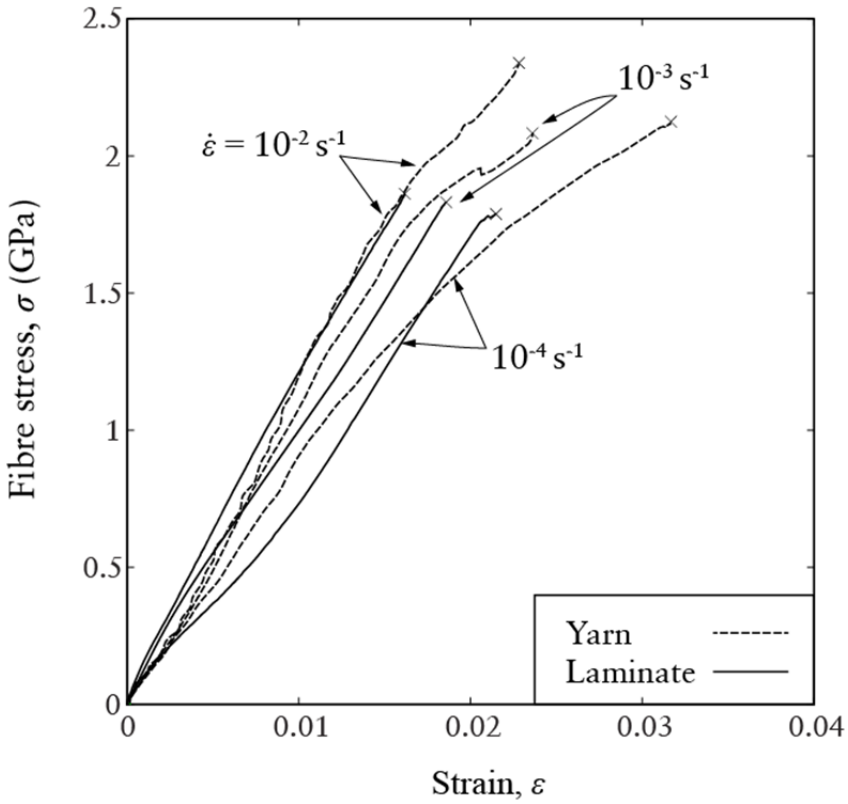


Fig. 9: Comparison of the stress versus strain responses for the SK76 yarn and HB26 laminate.

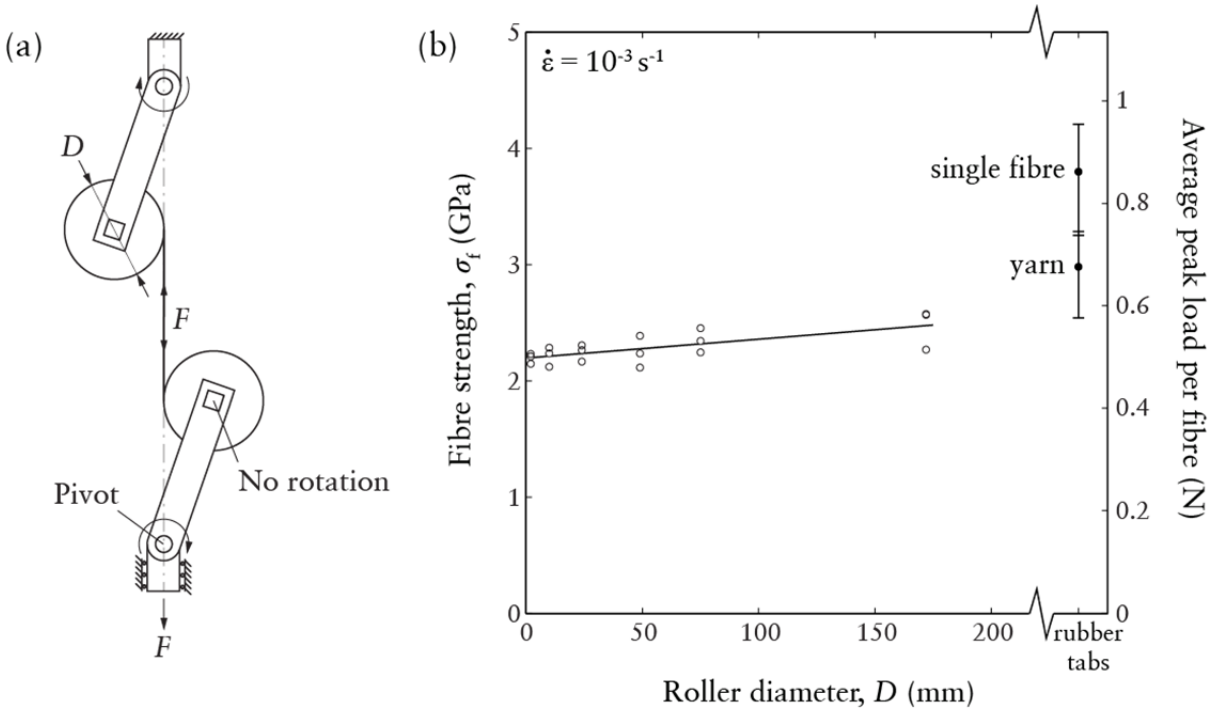


Fig. 10: SK76 yarn tests using a range of roller diameters. (a) Test set-up, (b) fibre strength versus roller diameter, *D* for a test strain rate of $10^{-3}$ s$^{-1}$. Data from rubber-tabbed specimens are included for a single fibre and a yarn.

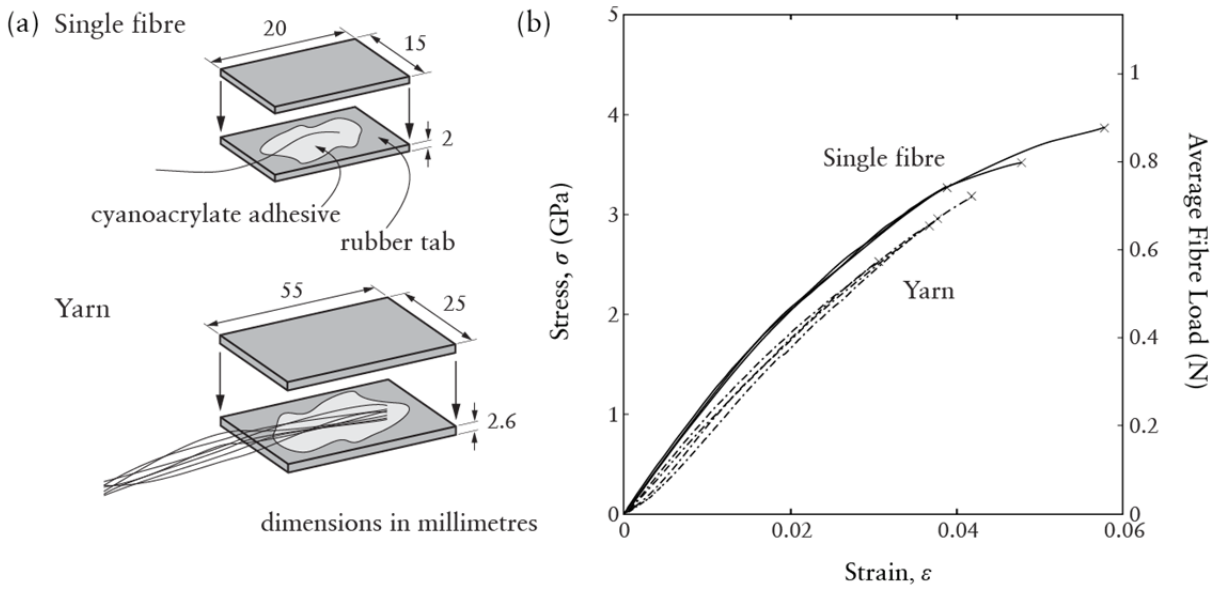


Fig. 11: (a) Sketch of the rubber end tab used for single fibre and yarn tensile tests. (b) The corresponding measured stress versus strain responses at a strain rate of $10^{-3}$ $s^{-1}$.